LA-UR- *09-03524*

Title:	Advances in Petascale Kinetic Plasma Simulation with VPIC and Roadrunner
Author(s):	K J Bowers, B J Albright, L Yin, B Daughton, V Roytershteyn and T J T Kwan
Intended for:	SCIDAC Conference Proceedings

Los Alamos
NATIONAL LABORATORY
—— EST.1943 ——

Advances in Petascale Kinetic Plasma Simulation with VPIC and Roadrunner

K J Bowers[1,4]**, B J Albright**[1]**, L Yin**[1]**, B Daughton**[1]**,
V Roytershteyn**[2]**, and T J T Kwan**[1]

[1] Applied Physics Division / Plasma Theory and Applications Group (-1-PTA)
[2] Theoretical Division / Applied Mathematics and Plasma Physics Group (T-5), Los Alamos National Laboratory, PO Box 1663, Los Alamos, NM, 87545

E-mail: kevin.j.bowers@gmail.com

Abstract. VPIC [1, 2], a first-principles 3d electromagnetic charge-conserving relativistic kinetic particle-in-cell (PIC) code, was recently adapted to run on Los Alamos's Roadrunner [3], the first supercomputer to break a petaflop (10^{15} floating point operations per second) in the TOP500 supercomputer performance rankings. [4] We give a brief overview of the modeling capabilities and optimization techniques used in VPIC and the computational characteristics of petascale supercomputers like Roadrunner. We then discuss three applications enabled by VPIC's unprecedented performance on Roadrunner: modeling laser plasma interaction in upcoming inertial confinement fusion experiments at the National Ignition Facility (NIF) [5,6], modeling short pulse laser GeV ion acceleration [7–10] and modeling reconnection in magnetic confinement fusion experiments [11].

1. Introduction

First-principles particle-in-cell (PIC) simulations [12, 13] are the only viable tool for understanding many plasma physics phenomena. PIC divides the simulation volume into a mesh of voxels (cells) and represents plasma as a large number of particles. These particles are "pushed" by mesh-sampled electric and magnetic fields. The fields in turn are updated using electrical currents "accumulated" from the particle motions. Though this is computationally expensive and, if implemented conventionally, inefficient on modern supercomputers, it gives insight into numerous phenomena impossible to measure directly or understand with more approximate methods.

Employing millions of voxels and billions of particles, large PIC simulations require large supercomputing resources. Due to physical limitations, moving data between and even within a supercomputer's microprocessors is more time consuming than performing even basic computations. Unfortunately, traditional PIC implementations, evolved from experience on vector supercomputers, require more data motion per computation than other methods often used in supercomputing (e.g., dense matrix, molecular dynamics N-body and Monte-Carlo calculations) and cannot utilize recently developed petascale supercomputers efficiently. Unlike traditional implementations, VPIC [1,2], a first-principles 3d electromagnetic charge-conserving

---

[4] Guest Scientist. Present adddress: D. E. Shaw Research LLC. 120 West 45th Street, 39th Floor, New York, NY 10036

relativistic kinetic PIC code, was designed from the ground up to minimize data motion. As a result, VPIC can more fully exploit the potential of petascale supercomputers, enabling simulations of numerous plasma physics phenomena at unmatched fidelity and scale—using over a trillion particles, a billion mesh points and/or a hundred thousand processing cores. VPIC running on Los Alamos's Roadrunner supercomputer is a prime example. In a parameter study of particle trapping physics within laser-driven hohlraums of inertial confinement fusion experiments [14], we measured end-to-end sustained performance exceeding 0.374 Pflop/s (s.p.) on 122,240 processing cores (17 of Roadrunner's 18 connected units) and performed simulations using over a trillion particles.

This paper is structured as follows: We give a brief overview of the modeleling capabilities and optimization techniques used in VPIC and the computational characteristics of Roadrunner. We then discuss three applications enabled by VPIC performance on Roadrunner: modeling laser-plasma interaction in upcoming inertial confinement fusion experiments at the National Ignition Facility (NIF) [5,6], modeling short-pulse laser GeV ion acceleration [7–10] and modeling magnetic reconnection in magnetic confinement fusion experiments [11].

2. VPIC on Roadrunner

In this section, we give a brief overview of VPIC and Roadrunner; ref. [1] and ref. [3] present modeling and computational capabilities, respectively, in greater detail. We also discuss recent VPIC developments.

2.1. VPIC Overview

VPIC integrates the relativistic Maxwell-Boltzmann equations in a linear background medium. To avoid a prohibitively costly discretization, VPIC samples the 6D position-momentum particle phase-space of each species with computational particles that follow the Boltzmann equation's characteristics. As a result, though computational particles typically represent many physical particles, their phase-space distribution obeys the Boltzmann equation outside of discrete particle collisional effects, which must be handled separately.

The time-dependent Maxwell equations and the particle equations of motion are integrated in time with a scheme based on a quasi-symplectic (e.g., phase-space volume conserving, when using lossless background materials and boundary conditions) Trotter factorization. The resulting timestep is an explicit-implicit mixture of leap-frog, Verlet, exponential differencing and Boris magnetic field rotations [15], modified to use a sixth-order rotation angle approximation [16]. The simulation domain is divided into a regular mesh of identical rectangular voxels with potentially irregular but mesh-aligned boundaries, with tens to thousands of particles per voxel. The electric and magnetic fields are sampled staggered on this mesh and interpolated to the particles with an "energy-conserving" scheme (i.e., consistent with a discretized energy principle). The curls of these fields are computed with second-order accurate finite differencing. The current density is sampled on the same mesh and extrapolated from the particles by the method of Villasenor and Buneman [17], making VPIC "charge-conserving" (i.e., in exact arithmetic, the fields satisfy an implied discretized continuity of charge relation). VPIC also infrequently applies Marder passes [18] tuned specifically to clean finite precision arithmetic error induced charge conservation violations. Relativistic particle motion can generate non-physical Cherenkov radiation in the discretized Maxwell equations; VPIC uses the charge-conserving transverse current adjustment method [19] to combat this.

Achieving high performance on modern supercomputers requires minimizing the number of internode communications, number of memory accesses, amount of data in internode communications, amount of memory accessed and number of arithmetic operations performed, in roughly that order. Fortunately, due to the finite c in relativistic simulations, internode communications are naturally optimized by VPIC's spatial domain decomposition. Thus, as

there is typically more field and particle data per node than can fit in any cache, DRAM access optimization is main technical challenge VPIC.

Key to this is the use of single precision. This allows the use of wider *single-instruction-multiple-data (SIMD)* instructions (e.g., four single precision operations can be processed simultaneously versus two double precision operations) while reducing data motion by half over double precision. For typical time steps, voxel dimensions and particles per voxel, model discretization error exceeds single precision arithmetic error and thus is acceptable provided it does not introduce other non-physical artifacts (e.g. large violations of otherwise conserved quantities in the simulation). To help ensure this, VPIC is stabilized against single precision arithmetic error. For example, particle coordinates are stored as a voxel index plus a normalized offset from the center of that voxel; this preserves various symmetries and gives orders of magnitude improvement in the worst case absolute position resolution over more conventional representations.

Also key is the heavily use of *streaming* memory access. For example, VPIC processes the majority of particles each timestep in a single pass. This, and storing the particle data contiguously and organized for efficient SIMD, means the particle update streams through the particles once using large aligned memory transfers. Likewise, to avoid randomly accessing field data each timestep, field interpolation coefficients for each voxel are precomputed before the particle update and saved in a contiguous SIMD compatible layout. Additionally, the particles are periodically sorted [20] such that all particles in a given voxel are processed approximately sequentially. The necessary field data for the particle advance is thus effectively streamed sequentially from memory into cache with large aligned memory transfers.

In the method of Villensor and Buneman [17], a particle makes a current contribution in each voxel through which it passes. To utilize SIMD here, VPIC exploits that particles do not cross voxel boundaries due to the finite c and simulation stability conditions. VPIC advances 4 particles simultaneously by assuming no boundary crossings occur. Particles that do cross are detected and are processed individually subsequently. Like the interpolation coefficients, current contributions in voxel are made to a contiguous SIMD compatible set of partial currents which is postprocessed into the current density before the field update. The same benefits described for interpolation coefficients apply. If a particle hits an "exceptional" boundary during current accumulation (e.g., needs to be sent to a neighboring node), the index and remaining particle displacement are saved to an exception list for later processing. This avoids additional passes through the particles to find exceptions.

2.2. Roadrunner overview

Roadrunner is a first-of-its-kind heterogeneous cluster-of-clusters at Los Alamos National Laboratory, utilizing $6,480$, 1.8 GHz, dual-core AMD Opteron CPUs and $12,960$, 3.2 GHz, IBM Cell eDP CPUs. Each Cell contains one general purpose *power processing element (PPE)* core and eight single precision 4-vector SIMD optimized *synergistic processing element (SPE)* cores. [21] Roadrunner's computational horsepower primarily resides in the SPEs, with an aggregate single precision theoretical peak performance of 2.7 Pflop/s. Unlike conventional cores, the SPEs cannot access memory directly. Rather, each SPE can only access 256 KiB of high performance *local store (LS)* specific to it. The LS is analogous to cache, but, unlike conventional cache, the SPE must explicitly manage DRAM transfers to and from the LS.

VPIC's performance is asymptotically limited by the rate particles can be streamed to and from DRAM. On Roadrunner, the SPE to Cell local DRAM bandwidth greatly exceeds the SPE to Opteron local DRAM bandwidth. Accordingly, on Roadrunner, all VPIC simulation state resides within Cell DRAM, the Cells are responsible for all computations and the Opterons manage communications among Cells. Initial porting effort focused on the dominant particle update kernel. Each SPE processes a fraction of the particles. A SPE triple-buffers its particles

in blocks of 512 (i.e., while a block is processed, the next is loaded and the previous is stored). To utilize SPE resources more fully, the SIMD loop used on conventional cores was hand unrolled by 4; effectively, each SPE processes 16 particles simultaneously. A custom 512 line software managed cache of voxel data handles random memory access. The cache has a fully-associative least-recently-used policy (i.e., a line can hold any voxel's data and the least recently used line is replaced when caching new data). As the last 512 requests are guaranteed to be cached, before processing a block, all needed voxel data is requested. Because particles are approximately sorted, most requests are already cached but the cache is sufficient to accomodate every particle in a different voxel. Overall, core-for-core and clock-for-clock, Roadrunner's SPE cores are faster than Roadrunner's Opteron cores and, in aggregate, the SPEs can process particles 15.6 times faster than the Opterons.

2.3. Recent VPIC Developments

To support model inertial confinement fusion LPI and thermonuclear burn modeling and magnetic fusion reconnection modeling, VPIC recently acquired four new modeling capabilities. First, the method of Ref. [22] is available to model elastic and inelastic short-range ion-ion collisions. In this, pairs of nearby particles are interacted to give a Monte-Carlo treatment of the Fokker-Planck collision operation in the Boltzmann equation. Second, the method of Ref. [23] is available to model ion-electron collisions. This uses a computationally inexpensive fluid model for the electrons, coupled to the ions by a stochastic Langevin process. Third, this fluid electron model was refined to incorporate electron-radiation coupling via ion-electron Bremsstrahlung, electron-electron Bremsstrahlung and Compton scattering processes. Lastly, additional particle boundary conditions appropriate for plasma inflows and outflows in magnetic reconnection are supported. [24].

Owing the the relative performance of the SPE and PPE cores, even minor kernels that do not exploit the SPEs are potential Amdahl bottlenecks. As such, recent computational efforts have focused on porting additional kernels to the SPEs. We first converted VPIC to use "overlays", allowing multiple kernels to share the limited SPE local store. Then, as performance is a balance between particle spatial organization (which improves the SPE's particle advance software cache performance) and the time spent organizing particles (the second most expensive operation overall), we ported VPIC's particle sorting to the SPEs.

The obvious implementation is a SPE-parallel version of the out-of-place counting sort described in Ref. [20]. In this, each SPE histograms a fraction of the particles by voxel. These histograms are converted into the sorted particle's partitioning by voxel and, using this partitioning, the SPEs make a copy of the particles in sorted order. For this method to scale, the conversion must also be SPE-parallel. Unfortunately, this requires large all-to-all exchanges among the SPEs within a Cell before and after the conversion. To avoid this, each SPE is first assigned a fraction of voxels and then particles are sorted by the SPE assigned the voxel containing the particle with a SPE-parallel out-of-place counting sort (given there are orders of magnitude fewer SPE than voxels, the conversion step involves a miniscule data exchange and need not be SPE-parallel). Next, noting that each SPE can now sort the particles in its assigned voxels completely independent, each SPE does a serial out-of-place counting sort of particles in its assigned voxels. We probe a few times more particles than there are SPE to estimate the optimal assignment of voxels to SPE to accomodate any particle non-uniformity. Overall, this requires $O(N_{particle}/N_{spe}) + O(N_{voxel}/N_{spe})$ operations, $O(N_{particle}) + O(N_{voxel})$ auxiliary storage.

We are currently SPE-parallelizing the field advance kernels. These kernels use a custom software managed cache to handle strided memory accesses, a simpler read-only 4-way set-associative protocol is sufficient. Many have already been done and, currently, the largest Amdahl bottlenecks often reside in one-off user-provided in-situ simulation diagnostics.
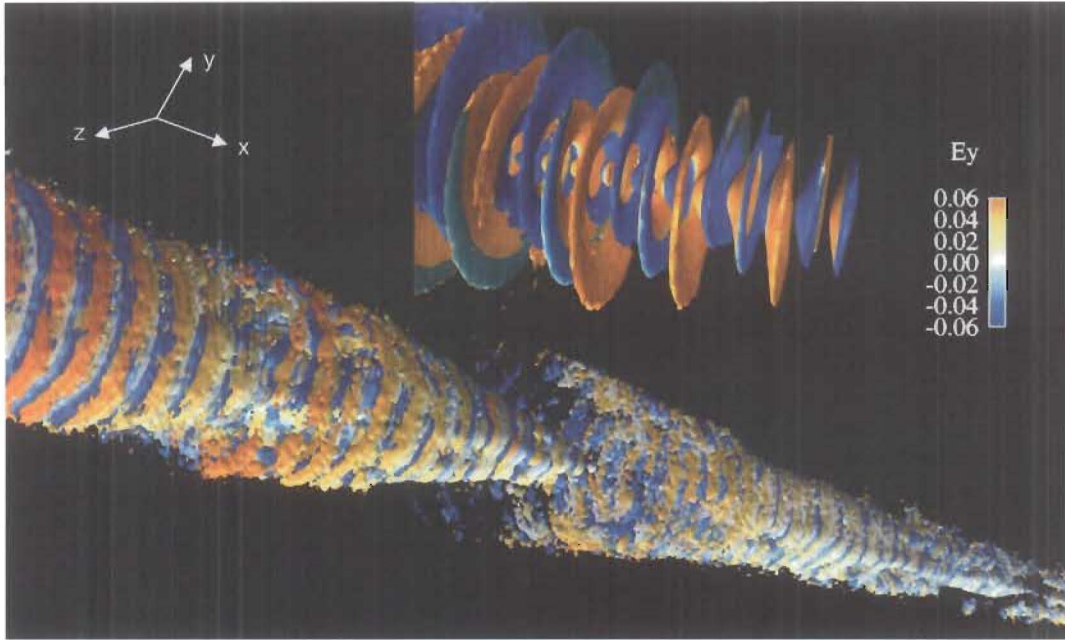
Figure 1. 3D VPIC LPI simulation under NIF plasma conditions. (Top) At SRS pulse saturation, the electron plasma wave excited by a f/4 laser speckle is bowing, causing the source for SRS laser backscatter to become incoherent. (Bottom) Owing to the larger speckle volume, the electron plasma wave produced in a f/8 speckle is also self-focusin and filamenting, further reducing backscatter. Isosurfaces of constant EPW electric field, colored by the laser electric field during SRS saturation are shown (color bar indicates the laser field strength in simulation units).

3. LPI Modeling of NIF Experiments

In 2010, inertial confinement fusion (ICF) experiments commence at the National Ignition Facility (NIF). In these, over a 10^6 Joules of laser energy is focused onto the inner walls of a gas-filled hohlraum, a hollow cylinder made of high-Z material such as gold or uranium. The hohlraum walls absorb the laser energy and re-radiate it as x-rays. These x-rays are absorbed by a spherical capsule at the hohlraum's center, causing the capsule—including deuterium-tritium fuel at its center—to compress, bringing the fuel to the high temperatures and pressures required for ignition of fusion reactions.

To prevent the hohlraum walls from ablating during the ~ 10 ns laser drive, a low-Z fill gas (H or He) is used. As the laser propagates, it ionizes this gas and laser-plasma instabilities (LPI), the stimulated scattering of laser light off plasma density fluctuations, may arise. LPI affect ICF experiments in three ways: they scatter laser light out of the hohlraum, reducing the energy delivered to the capsule; they scatter laser light to other places in the hohlraum, degrading capsule implosion symmetry; and, they pre-heat the fuel with hot electrons, making compression harder.

Stimulated Raman scattering (SRS), the resonant amplification of electron density fluctuations by a laser, is the greatest LPI concern in ICF. In ICF experiments, a roughly uniform laser intensity is maintained across the beam with random phase plates that break the beam into an ensemble of *laser speckles*. In a speckle, SRS manifests as the amplification of a forward directed *electron plasma wave (EPW)* and the backward scattering of laser light.

While the linear growth of SRS is well understood [25], single speckle experiments at the LANL Trident Laser facility evince nonlinear behavior: at a threshold intensity, SRS reflectivity rises abruptly to a level orders of magnitude higher than linear theory predicts. Above this threshold, reflectivity is laser drive intensity independent [26].

Recent work [5, 6] using VPIC has identified the essential nonlinear physics governing SRS under NIF-hohlraum conditions. Versus time, the scattering manifests as a series of pulses, each of which passes through 4 distinct phases: (1) SRS grows linearly from density fluctuations. (2) Electrons trapped by the EPW reduce the EPW frequency and phase velocity by an amount that scales with EPW amplitude. (3) Near the center of the speckle, where the amplitude is highest, the EPW phase velocity is lower than at the speckle's edge; EPW phase front bending ensues. (4) The EPW wave amplitude exceeds the electron's *trapped particle modulation instability (TPMI)* threshhold [27, 28]. TPMI generates waves off-axis from the laser direction and leads to EPW filamentation, self-focusing, and phase front breakup. Moreover, filamentation leads to increased trapped-electron transverse-loss, rapidly increasing EPW damping. As the source for SRS backscatter is proportional the product of the EPW and laser electric fields integrated over the speckle cross section [29], combined these terminate the pulse, fundamentally limiting speckle SRS backscatter.

Figure 1 (top) shows the effect of bowing. This snapshot was taken from a 3D VPIC LPI simulation at SRS pulse saturation of a f/4 beam with intensity $I_0 = 2.5 \times 10^{16}$ W/cm^2 under NIF plasma conditions in the trapping regime ($k\lambda_{De} = 0.34$, where k is the initial EPW wavenumber and λ_D is the Debye length). As bowing causes the EPW electric field's phase (but not amplitude) to change across the speckle, iso-surfaces of EPW electric field depict this bowing. The iso-surfaces are colored by the laser electric field intensity, graphically showing the how the source for SRS backscatter has become incoherent.

Figure 1 (bottom) shows the effects of self-focusing and filamentation. This snapshot was taken from a 3D VPIC LPI simulation of a f/8 beam with intesity $I_0 = 1.0 \times 10^{16}$ W/cm^2 and wave number $k\lambda_{De} = 0.34$. The speckle volume is 16 times larger than the previous simulation (325 billion particles on a $8256 \times 512 \times 512$ mesh were used), permitting a wider range of transverse self-focusing modes to develop. This leads to chaotic phase variation across the speckle and the EPW filamentation (this process does not occur in a f/4 speckle as angular symmetry is approximately maintained). This further reduces SRS source coherence and increases wave damping, quenching the SRS pulse.

Current research is investigating whether neighboring speckles can interact with one another via exchange of hot electrons or waves to produce higher backscatter than the speckles would individually. Earlier work [30] showed that hot electrons from one speckle can destabilize a neighboring speckle and lower the threshold for nonlinear SRS under some conditions. However, this work employed 2D simulations, over-predicting the amount of hot electron communication. 3D petascale *ab initio* VPIC simulations on Roadrunner are necessary to examine this problem quantitatively.

4. GeV Ion Acceleration using Short-Pulse Lasers and Nano-Scale Targets
This past decade has seen an explosion of interest in charged particle acceleration via the interaction of ultra-intense ($I > 10^{18}$ W/cm^2) short-pulse (~ps) lasers with plasma. When such a laser strikes a ~ 10s of micron thick solid-density target, hot electrons are produced on where the laser is absorbed, travel through the target and create a *sheath* on the rear target surface with very large (~TV/m) electric fields. These fields ionize and accelerate ions on the rear surface in the *target-normal sheath acceleration (TNSA)* process [31, 32]. The resulting ion beams have current orders of magnitude higher than conventional accelerators and transverse emittance orders of magnitude lower. With careful target preparation, the TNSA mechanism has been shown in experiments [33] and in VPIC simulations and analytic theory [7] to generate
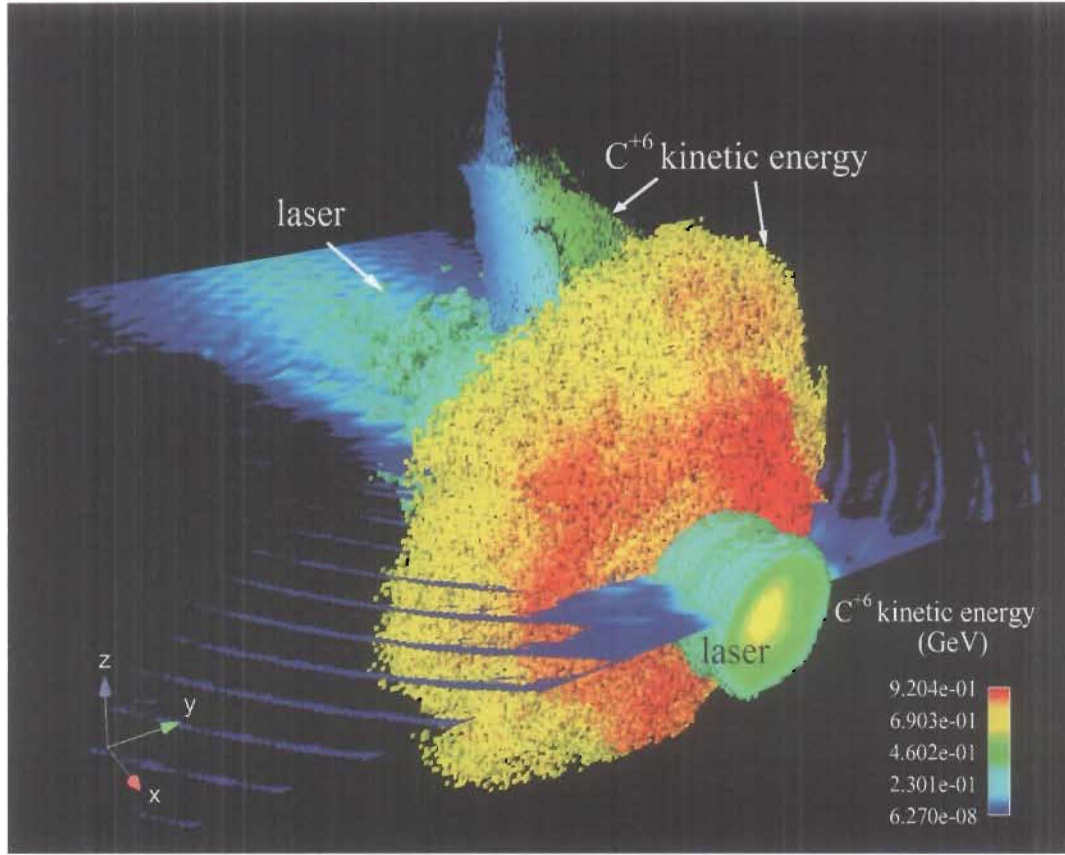
Figure 2. 3D VPIC simulation of ion acceleration using circular polarized laser light at intensity $I_0 \simeq 10^{21}$ W/cm^2 incident on a 30 nm C^{6+} target. The resulting peak ion energy is approaching GeV, as indicated by the iso-surface of red-yellow color.

quasi-monoenergetic ion beam spectra.

Ultra-intense lasers with contrast exceeding 10^{10} permit the use of nano-scale targets without the laser pre-pulse destroying the target. VPIC simulations [8,9] showed in such a configuration that the target can become relativistically transparent to the laser. As the laser penetrates the target, a brief period of enhanced acceleration, the *Break-out Afterburner (BOA)*, ensues, possibly as a result of a relativistic Buneman instability [10]. This leads to enhanced ion beam energy and laser-to-ion-beam energy conversion efficiency.

In addition to the BOA, which uses a linearly polarized laser, others [34] have examined the use of ultra-high contrast circularly polarized lasers. In this regime, radiation pressure accelerates the ions instead of a plasma instability and 3D VPIC simulations on Roadrunner confirmed this analysis. Figure 2 shows ion acceleration using a 30 nm C6$^+$ target at solid density $n_e/n_{cr} = 660$, where n_{cr} is the critical density for laser absorption, and a 312 fs laser pulse of peak intensity of $I_0 \simeq 10^{21}$ W/cm^2. Acceleration of C6$^+$ ions is shown at when the laser has penetrated the target; the maximum ion energy is approaching a GeV. This simulation used 14×10^9 cells and 21×10^9 particles; simulations of such a solid density target over an such extended domain is not possible without petascale resources like VPIC on Roadrunner.

As high-energy ion beam generation using ultra-thin targets and two different ion acceleration

mechanisms (laser polarizations) at moderately-high laser intensity yielded promising results, current investigations are exploring even higher laser intensities and optimizing the laser pulse length, target composition and thickness for ¿GeV proton beam generation.

5. Magnetic Reconnection

In magnetic reconnection, magnetic field energy is rapidly converted into kinetic energy, including high speed particle flows, ion and electron thermal heating and highly energetic non-thermal tails. Reconnection is ubiquitous in plasma physics, occuring in tokamak devices, planetary magnetospheres, solar flares, extragalactic jets and a wide variety of other settings, yet poorly understood. In collisional regimes, magnetohydrodynamics (MHD) gives a reasonable model, but, in weakly collisional regimes, theoretical models and fluid simulations have been unsatisfactory. VPIC's new collisional modeling capabilities permit a direct solution of the full plasma kinetic equation, the theoretical basis for reduced models like MHD. This approach allows rigorous study of the reconnection at arbitrary collisionality [11], covering both the fluid and kinetic regimes.

Reconnection simulations are challenging due to the widely separated space and time scales involved. High temperature plasmas are good conductors, implying they trap magnetic flux for very long times. During reconnection, this *frozen-flux* condition is rapidly broken within very small *diffusion* regions. Our present research aims to understand diffusion region dynamics and the coupling between diffusion regions and macroscopic scales. To that end, VPIC simulations on Roadrunner are (1) modeling a well-diagnosed laboratory reconnection experiment in a semi-collisional regime and (2) modeling large-scale collisionless reconnection layers in Earth's magnetosphere.

The Magnetic Reconnection eXperiment (MRX) recently reported detailed measurements of the diffusion region, including the electron layer's kinetic structure [35]. MRX's reconnection is driven by reducing the current within two axi-symmetric flux cores. This was recently modeled using a 2D collisionless PIC code with boundary conditions appropriate to the actual experiment [36]. Although this demonstrated a number of striking similarities for ion scale structures, the experimentally measured electron layer thickness was $3-5\times$ larger than observed in the 2D simulation [37]. Two possibilities for this discrepancy, weak Coulomb collisions and 3D effects (e.g., plasma instabilities within the electron layer), are being investigated with VPIC. Collisional 2D VPIC simulations yield significantly broader electron layers and allow uncertain experimental parameters, such as the electron temperature, to be estimated under the assumption layer broadening is due to Coulomb collisions alone. Preliminary 3D simulations in the collisionless limit have also demonstrated plasma instabilities within the electron layer. Figure 3 (top), taken from one of these 3D simulations, shows the flux cores, magnetic field structure, ion outflow and electron current sheet.

Modeling large-scale reconnection in Earth's magnetosphere presents additional challenges: the plasma is highly collisionless and the ion kinetic scales are nearly $100\times$ larger than the MRX device. But simulations focusing about a reconnection site are still within reach. These simulations employ an open boundary model [24], allowing both magnetic flux and plasma to enter and exit the system—avoiding unphysical recirculation effects that quickly dominate periodic simulations. A zero derivative condition on the time averaged particle moments up through the pressure tensor is employed on plasma outflows and an absorbing Higdon [38] boundary condition is used for the fields. Plasma inflows, at a density and temperature appropriate for the solar wind, are prescribed by the simulation electric field. Figure 3 (bottom) magnetic island formation along the resonant surfaces across the initial current sheet. In 3D, these islands form extended flux ropes at oblique angles above and below the reconnection layer. Over longer time scales, these flux ropes coalesce and intertwine in complex ways and produce new highly elongated current sheets, which are also unstable to the formation of new magnetic
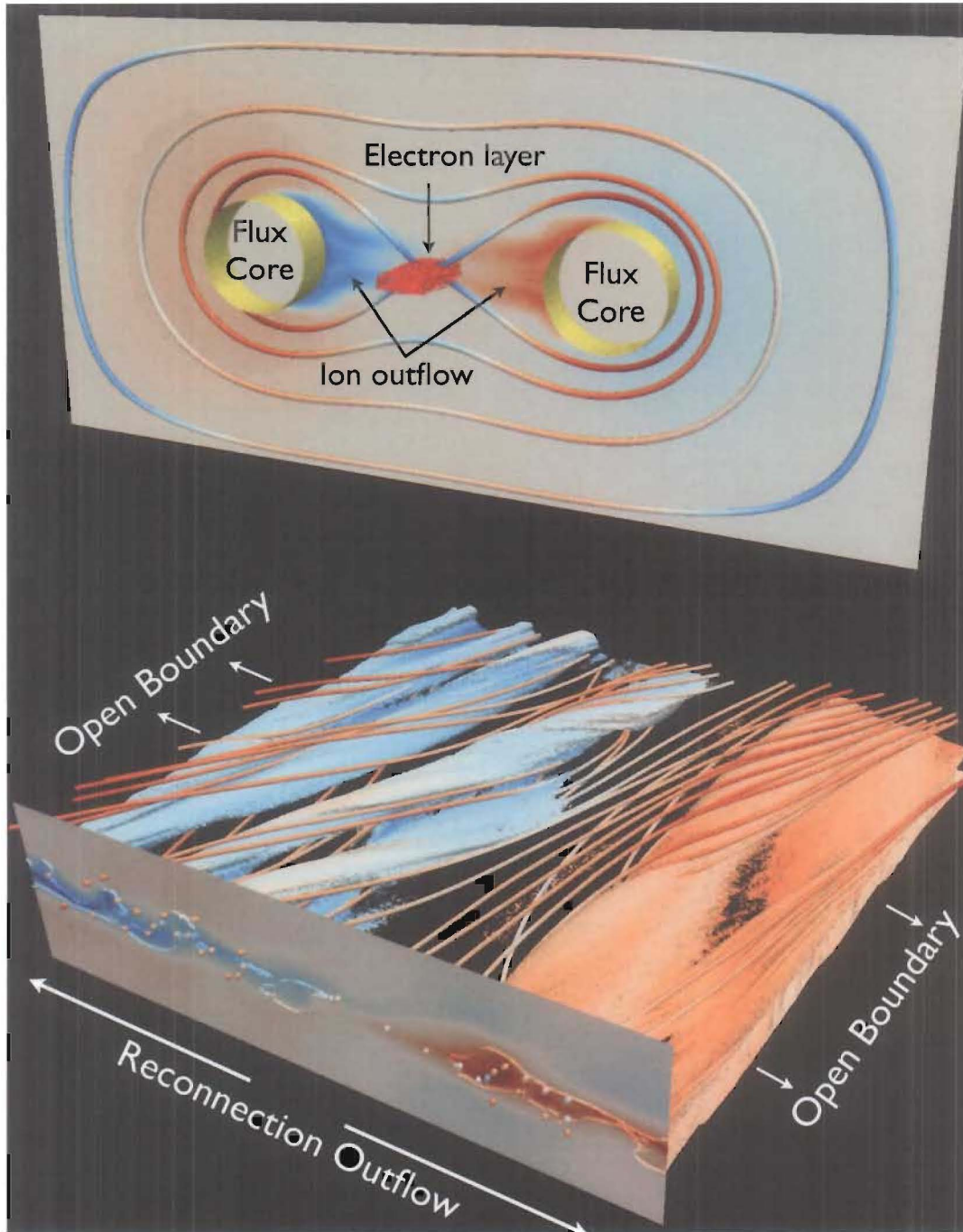
Figure 3. (Top)2D collisional simulation of reconnection in MRX uses two flux cores; reconnection is driven by reducing the current within the flux cores like the experiment. (Bottom)3D simulation of reconnection in Earth's magnetosphere. Open boundary conditions allow plasma and magnetic flux to enter and exit the system. Shown is a density isosurface colored by the ion outflow velocity along magnetic field lines.

islands (flux ropes).

References
[1] Bowers K J, Albright B J, Yin L, Bergen B and Kwan T J T 2008 *Phys. Plasmas* **15** 055703
[2] Bowers K J *Proceedings of the International Conference on the Numerical Simulation of Plasmas*
[3] Bowers K J, Albright B J, Bergen B, Yin L, Barker K J and Kerbyson D J 2008 *SC '08: Proceedings of the 2008 ACM/IEEE conference on Supercomputing* (Piscataway, NJ, USA: IEEE Press) pp 1–11
[4] Dongarra J Top500 supercomputers, *http://www.top500.org* URL www.top500.org
[5] Yin L, Albright B J, Bowers K J, Daughton W and Rose H A 2007 *Phys. Rev. Lett.* **99**
[6] Yin L, Albright B J, Bowers K J, Daughton W and Rose H A 2008 *Phys. Plasmas* **15**
[7] Albright B J, Yin L, Hegelich B M, Bowers K J, Kwan T J T and Fernández J C 2006 *Phys. Rev. Lett.* **97**
[8] Yin L, Albright B J, Hegelich B M and Fernández J C 2006 *Laser and Particle Beams* **24** 291
[9] Yin L, Albright B J, Hegelich B M, Bowers K J, Flippo K A, Kwan T J T and Fernández J C 2007 *Phys. Plasmas* **14** 056506
[10] Albright B J, Yin L, Bowers K J, Hegelich B M, Flippo K A, Kwan T J T and Fernández J C 2007 *Phys. Plasmas* **14** 094502
[11] Daughton W, Roytershteyn V, Albright B J, Karimabadi H, Yin L and Bowers K J 2009 *Phys. Plasmas, to appear*
[12] Birdsall C K and Langdon A B 1985 *Plasma Physics via Computer Simulation* (New York, NY: McGraw-Hill Inc.)
[13] Hockney R W and Eastwood J W 1988 *Computer Simulation Using Particles* (Philadelphia, PA: Institute of Physics Publishing)
[14] Albright B J, Bowers K J, Yin L, Bergen B, Daughton W, Kwan T J T, Snell C, Hegelich B M, Flippo K and Fernández J C High performance modeling of laser-plasma interaction in the era of petascale computing proceedings of the 13th Advanced Accelerator Concepts Workshop, July 27–Aug. 28, Santa Cruz, California, USA
[15] Boris J P 1970 *Proceedings of the 4th Conference on Numerical Simulation of Plasmas* ed Boris J P and Shanny R A (Washington D. C.: Naval Research Laboratory) pp 3–67
[16] Blahovec J D, Bowers L A, Luginsland J W, Sasser G E and Watrous J J 2000 *IEEE Trans. Plasma Sci.* **28** 821–829
[17] Villasenor J and Buneman O 1992 *Comp. Phys. Comm.* **69** 306–316
[18] Marder B 1987 *J. Comp. Phys.* **68** 48–55
[19] Eastwood J W, Arter W, Brealey N J and Hockney R W 1995 *Comp. Phys. Comm.* **87** 155–178
[20] Bowers K J 2001 *J. Comp. Phys.* **173** 393–411
[21] Kahle J A, Day M N, Hofstee H P, Johns C R, Maeurer T R and Shippy D 2005 *IBM J. Res. Dev.* **49**
[22] Takizuka T and Abe H 1977 *J. Comp. Phys.* **25** 205
[23] Lemons D S, Winske D, Daughton W and Albright B J 2009 *J. Comp. Phys.* **228** 1391–1403
[24] Daughton W, Scudder J and Karimabadi H 2006 *Phys. Plasmas* **13** 072101
[25] Drake J F, Kaw P K, Lee Y C, Schmid G, Liu C S and Rosenbluth M N 1974 *Phys. Fluids* **17** 778
[26] Montgomery D S, Cobble J A, Fernández J C, Focia R J, Johnson R P, Renard-LeGalloudec N, Rose H A and Russell D A 2002 *Phys. Plasmas* **9** 2311 2320
[27] Rose H A 2005 *Phys. Plasmas* **12** 012318
[28] Rose H A and Yin L 2008 *Phys. Plasmas* **15** 042311
[29] Russell D A, DuBois D F and Rose H A 1999 *Phys. Plasmas* **6** 1294–1317
[30] Albright B J, Daughton W, Yin L, Bowers K J, Kline J L, Montgomery D S and Fernández J C *J. Phys. IV* **133** 253
[31] Hatchett S P, Brown C G, Cowan T E, Henry E A, Johnson J S, Key M H, Koch J A, Langdon A B, Lasinski B F, Lee R W, Mackinnon A J, Pennington D M, Perry M D, Phillips T W, Roth M, Sangster T C, Singh M S, Snavely R A, Stoyer M A, Wilks S C and Yasuike K 2000 *Phys. Plasmas* **7** 2076–2082
[32] Maksimchuk A, Gu S, Flippo K, Umstadter D and Bychenkov V Y 2000 *Phys. Rev. Lett.* **84** 4108–4111

[33] Hegelich B M, Albright B J, Cobble J, Flippo K, Letzring S, Paffett M, Ruhl H, Schreiber J, Schulze R K and Fernández J C 2006 *Nature* **439** 441–444
[34] Robinson A P L, Zeph M, Kar S, Evans R G and Bellei C 2008 *New Journal of Physics* **10** 013021
[35] Ren Y, Yamada M, Ji H, Dorfman S, Gerhardt S P and Kulsrud R
[36] Dorfman S, Daughton W, Roytershteyn V, Ji H, Ren Y and Yamada M 2008 *Phys. Plasmas* **15** 102107
[37] Ji H, Ren Y, Yamada M, Dorfman S, Daughton W and Gerhardt S P 2008 *Geophys. Res. Lett.* **35**
[38] Higdon R L 1986 *Mathematics of Computation* **47** 437–459